Third-Eye: A Mobilephone-Enabled Crowdsensing System for Air Quality Monitoring

LIANG LIU[1], WU LIU[1], YU ZHENG[2], HUADONG MA[1], CHENG ZHANG[1*],
[1] Beijing Key Laboratory of Intelligent Telecommunications Software and Multimedia,
Beijing University of Posts and Telecommunications, Beijing 10086, China
[2] Microsoft Research Asia, Beijing 100080, China

Air pollution has raised people's public health concerns in major cities, especially for Particulate Matter under $2.5\mu m$ ($PM_{2.5}$) due to its significant impact on human respiratory and circulation systems. In this paper, we present the design, implementation, and evaluation of a mobile application, Third-Eye, that can turn mobile phones into high-quality $PM_{2.5}$ monitors, thereby enabling a crowdsensing way for fine-grained $PM_{2.5}$ monitoring in the city. We explore two ways, crowdsensing and web crawling, to efficiently build large-scale datasets of the outdoor images taken by mobile phone, weather data, and air-pollution data. Then, we leverage two deep learning models, Convolutional Neural Network (CNN) for images and Long Short Term Memory (LSTM) network for weather and air-pollution data, to build an end-to-end framework for training $PM_{2.5}$ inference models. Our App has been downloaded more than 2,000 times and runs more than 1 year. The real user data based evaluation shows that Third-Eye achieves 17.38 $\mu g/m^3$ average error and 81.55% classification accuracy, which outperforms 5 state-of-the-art methods, including three scattered interpolations and two image based estimation methods. The results also demonstrate how Third-Eye offers substantial enhancements over typical portable $PM_{2.5}$ monitors by simultaneously improving accessibility, portability, and accuracy.

CCS Concepts: • **Human-centered computing** → **Ubiquitous and mobile computing**;

Additional Key Words and Phrases: Air quality, $PM_{2.5}$ monitoring, crowdsensing, CNN, LSTM

ACM Reference Format:
Liang Liu[1], Wu Liu[1], Yu Zheng[2], Huadong Ma[1], Cheng Zhang[1]. 2018. Third-Eye: A Mobilephone-Enabled Crowdsensing System for Air Quality Monitoring. *Proc. ACM Interact. Mob. Wearable Ubiquitous Technol.* 2, 1, Article 20 (March 2018), 26 pages.
https://doi.org/10.1145/3191752

1 INTRODUCTION

Rapid urbanization results in severe air pollution problem, especially for cities in developing countries. Air quality monitoring is of great importance to support air pollution control and protect humans

*Authors' addresses: Liang Liu, Wu Liu, Huadong Ma, and Cheng Zhang, Box 139, No.10 Xitucheng Road, Haidian District, Beijing 100876, China, {liangliu, liuwu, mhd, zhangcheng}@bupt.edu.cn; Yu Zheng, Building 2, No.5 Danling Street, Haidian District, Beijing 100080, China, yuzheng@outlook.com.

Permission to make digital or hard copies of all or part of this work for personal or classroom use is granted without fee provided that copies are not made or distributed for profit or commercial advantage and that copies bear this notice and the full citation on the first page. Copyrights for components of this work owned by others than ACM must be honored. Abstracting with credit is permitted. To copy otherwise, or republish, to post on servers or to redistribute to lists, requires prior specific permission and/or a fee. Request permissions from permissions@acm.org.
© 2018 Association for Computing Machinery.
2474-9567/2018/3-ART20 $$15.00
https://doi.org/10.1145/3191752

(a) (b) (c)

Fig. 1. (a) Air quality monitoring site; (b) portable $PM_{2.5}$ monitor; (c) mobile phone camera enabled $PM_{2.5}$ monitoring.

from damage by air pollution. As a typical indicator for urban air quality, $PM_{2.5}$ (particulate matter with a diameter of 2.5 micrometers or less), has gained considerable attention recently because of its significant impact on people's respiratory systems [3] and even circulation systems [22]. Understanding the consequences of urban $PM_{2.5}$ change will require an effort of comprehensive long-term data collection and synthesis that mainly relies on networked monitoring sites. However, the monitoring sites are usually insufficient such that it is difficult to obtain fine-grained city wide $PM_{2.5}$ status over the whole city. Take Beijing for example, only 35 sites are deployed in the $16,000$ km^2 region, i.e., 457 km^2 per site. As demonstrated in Fig. 1(a), an air quality monitoring site usually requires a large land of foortprint with non-trivial money (about 200,000 USD for construction and 30,000 USD per year for maintenance) and labor efforts [32].

In order to obtain fine-grained data, it is necessary to infer a location's $PM_{2.5}$ without monitoring sites. Scattered interpolation is a typical method that uses spatial variance signals' in order to infer missing information. However, existing research reveals that $PM_{2.5}$ has considerable spatial variations. Paper [32] finds that the $PM_{2.5}$ reported by stations are quite different sometimes though they are geospatially close. It further illustrates the distribution of the deviation among 22 stations in Beijing over 3 months (Feb. 8 to May 27, 2013). Over 39 percent of the cases have a deviation greater than 100. We also analyze 15 months' $PM_{2.5}$ data (Jun. 21, 2016 to Sep. 23, 2017) which comes from 14 sites in the main city of Beijing. The average distance among the 14 sites is $9.4km$. Each site generates one $PM_{2.5}$ record per hour. We calculate the maximum deviation and the standard deviation of the 14 sites' data per day. The results are illustrated in Fig. 2. The average maximum deviation and standard deviation are 147.80 and 30.94, respectively. Our results also demonstrate the dynamic nature of $PM_{2.5}$ in urban spaces.

Thus, the sparse and preferentially located monitoring sites make spatial interpolation inaccurate in many cases. From the urban perspective, it is urgent to develop new monitoring techniques for effectively generating fine-grained $PM_{2.5}$ data with high accuracy. From the individual perspective, the sparse sites also lead to the release of publicly-available $PM_{2.5}$ data at the city-space or district-level that cannot measure the quality of the actual air quality that people breathe in. As a result, people need a new way to obtain reliable and accurate measurement of $PM_{2.5}$ in their immediate environment. That also can help users to take appropriate actions. For example, a runner may stay at home if the current $PM_{2.5}$ reading is too high; and a man who has respiratory disease may wear a surgical mask once the current $PM_{2.5}$ concentration exceeds a threshold.

Mobile sensing or crowdsensing [11, 13, 18], a new concept in ubiquitous computing where every owner of a portable sensing device in an urban area can be regarded as a sensing component, has brought us to a tipping point in the field of urban sensing. With development of embedded technology

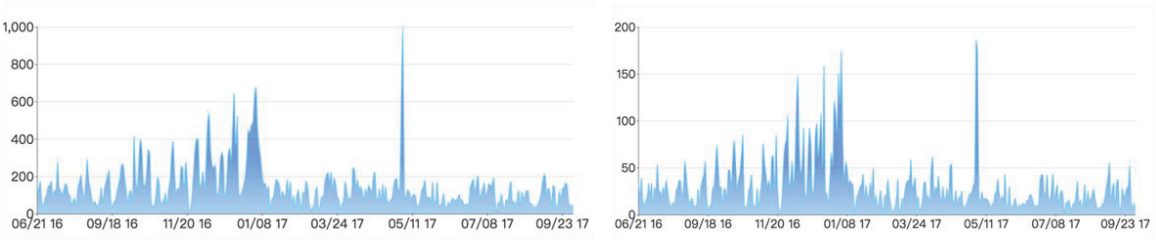

(a) Maximum Deviation

(b) Standard Deviation

Fig. 2. Statistical results of 15 months' $PM_{2.5}$ data from 14 sites in the main city of Beijing (June 21, 2016 to Sep. 23, 2017).

and the miniaturization of air quality sensors, several manufacturers such as Dylos and Aeroqual have recently introduced handheld devices. These devices can be carried by pedestrians for personal use and measure main air pollutants including $PM_{2.5}$. However, crowdsensing of $PM_{2.5}$ data is facing a bottleneck: the measurement quality of portable devices is relatively low. High-quality measurement is achieved by both high-precision sensors and strict measurement rules. As shown in Fig. 1(a), devices for accurate sensing of $PM_{2.5}$ are not portable. In addition, these devices need long periods of sensing time (e.g., 1 hour) before generating accurate results. In contrast, considering the factors of cost and size, many sensors in consumer portable devices have large errors. Moreover, it is difficult to guarantee that device owners follow professional measurement rules. We collected 3 months' $PM_{2.5}$ data nearby a monitoring site in Beijing using Dylos 1700 (see Fig. 1(b)) that is extensively used in research of $PM_{2.5}$ crowdsensing [6, 12, 24]. Compared the measurements of Dylos 1700 with the monitoring site's data which can be regarded as ground truth, the average error is as high as 43.4 (the unit of $PM_{2.5}$ is $\mu g\ m^3$ in the entire paper). Besides low quality measurement, another shortage is that the crowdsensing participant needs to carry around a special device that adds extra burden for participants. The size of Dylos 1700 is 178mm ×114mm×76mm, and the weight is 544g. Very few people want to carry around such device when they go out.

This paper aims to provide people a convenient way to determine the real-time $PM_{2.5}$ concentrations of their current locations, while provide cities with a means to crowdsense fine-grained $PM_{2.5}$ measurement. In order to achieve this goal, however, we face three specific challenges.

The first challenge is *how to design a truly portable $PM_{2.5}$ monitoring device for users?* Inspired by existing works about image based visibility or haze level analysis in the field of image processing [14, 21], we utilize mobile phone photos taken from outdoors to estimate the $PM_{2.5}$ concentration (see Fig. 1(c)). That means a mobilephone camera serves as the $PM_{2.5}$ sensor on the basis of the physical principle that light intensity attenuates because of the particulate matter scattering. Based on the *dark channel prior* which has been well studied in the field of image haze removal [14], we utilize pairs of dark channel image and $PM_{2.5}$ ground truth to train both regression and classification models. The regression error is 33.81 and the classification accuracy is 61.52%.[1]

The second challenge is *how to further promote the quality of mobile phone based $PM_{2.5}$ monitoring?* According to existing studies [25, 27], some other categories of data, such as the weather, traffic flow, and road networks, strongly correlate with air quality. In prior work by Zheng [32], these data are coupled with machine learning and data mining techniques to infer fine-grained air quality. After that,

[1]By reference to the international AQI standard, we set 6 levels of $PM_{2.5}$ concentration.

some studies [6, 19] attempt to predict and monitor air quality from various data sources, ranging from deployed physical sensors to social media. In this paper, we also find that $PM_{2.5}$ is highly related to other kinds of air-pollution data, such as NO_2, CO, SO_2, and O_3 levels. Thus, we combine weather data and air-pollution data (W&A data for short) to assist $PM_{2.5}$ inference. Considering the correlation may have a delayed effect (i.e., the current $PM_{2.5}$ may be affected by the weather and air-pollution conditions several hours ago), we use 48 hours' W&A data (include the current hour and prior 47 hours) to construct a vector sequence, and then train the regression and classification models which achieve 22.06 regression error and 78.29% classification accuracy, respectively. After fusing the results from the image based model and W&A data based model, the final result achieves 17.38 average error and 81.55% classification accuracy.

The third challenge is *how to design a concise and practical machine learning framework to train these models?* Theoretically speaking, the more kinds of correlated data utilized for training, the better inference results would be achieved. But it also becomes more difficult for modeling the correlation among a variety of data sources, as it relies on sophisticated models, well-designed features, mass training data, and costly calculation. For a practical application, it is important to tradeoff inference accuracy, conciseness, efficiency, and economy. Therefore, we choose the outdoor image data, weather data, and air-pollution data, which are easily obtained by mobile phone users or on the Internet. We also design two solutions, crowdsensing and web crawling, to efficiently collect large-scale data and automatically generate labeled training data. We further exploit two well-known deep learning models, *convolutional neural network* (CNN) for image data and *long short term memory network* (LSTM) for W&A data, to provide an end-to-end framework for training models with little pre/post-processing.

The contribution of this paper lies in the following four aspects:

- Framework. The proposed framework performs $PM_{2.5}$ concentration inference across Beijing, China, using outdoor-images and temporally-related weather/air-pollutant data. Moreover, our framework provides a complete solution including dataset generation, offline learning, and online inference. It exploits two phases crowdsensing - one phase for crowdsensing training dataset, and the other for crowdsensing fine-grained $PM_{2.5}$ situation over the city. This framework contributes to not only the $PM_{2.5}$ monitoring application but also the general problem of air quality inference.
- Model. We utilize CNN and LSTM to model the dark channel image and weather/air factors that influence $PM_{2.5}$. By directly learning an end-to-end models from these data, the network provides a concise and practical solution with little pre/post-processing.
- Dataset. We collected 31,601 labeled outdoor images around 8 monitoring sites in Beijing over one year. To the best of our knowledge, this is the largest outdoor images dataset for air quality inference. We also build a dataset of weather/air-pollution in Beijing which includes more than 150,000 records.
- Application. We develop an APP (including three versions for Android, iOS, and WeChat) for mobilephone users in Beijing. It has been downloaded more than 2,000 times. User data analysis verify that our APP outperforms 5 state-of-the-art methods and 4 popular portable devices.

We name our APP "Third-eye" which is a mystical and esoteric concept of a speculative invisible eye which provides perception beyond ordinary sight. This name implies that this APP could make the mobilephone's camera become the third eye of people which is able to see $PM_{2.5}$ value. This study is useful for helping realize real-time monitoring, analysis and pre-warning of $PM_{2.5}$ and it also helps to broaden the application of crowdsensing and the multi-source data mining methods.

2 RELATED WORK

This study is closely related to multiple research fields, ranging from sensor technology, data mining, and image processing. We group related studies into three categories and survey the literature in detail.

2.1 Portable Device Based Crowdsensing

Air quality monitoring is a typical application of crowdsensing. In the early studies, as a mobile platform, vehicles are commonly used to carry air quality devices. The authors of [1] designed a wireless distributed mobile air pollution monitoring system which utilized city buses with air pollution sensors array to collect pollutant gases (e.g., CO, NO_2, and SO_2) in the city of Sharjah, UAE. The authors of [2] built an environmental air quality sensing system and deployed it on street sweeping vehicles to monitor air quality in San Fransisco. The authors of [8] presented a vehicular-based mobile approach for realtime pollution measurement (dust concentration and Carbon monoxide concentrations). They desinged a mobile sensing box, deployable on public transportation and a personal sensing device (NODE) that can be used to create a social pollution sensing. These works did not collect the $PM_{2.5}$ data as it is difficult to be measured.

Recently, various attempts have been made to design and employ low-cost portable $PM_{2.5}$ monitor to achieve fine-grained sensory data. The authors of [6] present a client-cloud system, for pervasive and personal air-quality monitoring at low cost. They proposed two types of $PM_{2.5}$ monitors, AQM and miniAQM, with designed mechanical structures for optimal air-flow. Based on a carefully tuned airflow structure and a GPS-assisted filtering method, the authors of [12] built a $PM_{2.5}$ monitoring device, Mosaic-Nodes, with a novel constructive airflow-disturbance design. They also deployed eight Mosaic-Nodes to the selected buses to collect air quality data in Hangzhou, China. The authors of [24] developed a personal and portable particle counter device under $50. Its design can be readily adapted into a range of form factors, including a small wrist worn device. The authors also conducted a preliminary user study to report on the overall user experience of this device.

However, these portable $PM_{2.5}$ monitors make users bring along additional devices. Even a small wrist worn device may cause the user much inconvenience in many cases. Accuracy is another bottleneck. Considering the factors of cost and size, many sensors in portable devices have large errors.

2.2 Multisource Data Based Inference

Compared with the direct monitoring approaches, the multisource data based inference approaches received more and more attention in the past of recent years. Because many other categories of data, which have strong correlations with air quality, can provide information source complementary to monitoring sites. The authors of [4] proposed a big spatio-temporal data framework for the analysis of China Severe Smog. They collected about 35,000,000 detailed historical and real-time air quality records (containing the concentrations of $PM_{2.5}$ and the other air pollutants including SO_2, CO, NO_2, O_3 and PM_{10}) and 30,000,000 meteorological records in 77 major cities of China through air quality and weather stations. It conducts scalable correlation analysis to find the possible short-term and long-term factors to $PM_{2.5}$. Based on the back propagation neural network model, the authors of [19] realized the correlation analysis of $PM_{2.5}$ concentrations in Beijing. They found that the value of average wind speed, the concentrations of CO, NO_2, PM_{10}, and the daily number of microblog entries with key words "Beijing; Air pollution" show high mathematical correlation with $PM_{2.5}$ concentrations.

In the prior work by Yu Zheng [32], a co-training-based semi-supervised learning approach is proposed to infer the fine-granularity air quality. This work is on the basis of the AQIs reported by a few air quality monitor stations and four datasets (meteorological data, taxi trajectories, road networks, and

POIs) observed in the city. Inspired by this work, the authors of [6] also created an air-quality analytics engine that learned and created models of air-quality based on a fusion of multisource data. This engine is used to calibrate AQMs and miniAQMs in real-time, and infers $PM_{2.5}$ concentrations.

The authors of [5] integrated social web data and device web data to build standard health hazard rating reference, and trained smog-health models for health hazard prediction. They applied the rating reference and models to online and location-sensitive smog disaster monitoring. In [8], the authors also proposed a method for air quality estimation from social media post such as Weibo text content based on a series of progressively more sophisticated machine learning models.

The authors of [23] presented a novel spatial interpolation framework to incorporate diverse data sources and model the spatial processes explicitly at multiple resolutions. For a set of heterogeneous data across different domains, spectral analysis is deployed to generate features at multiple spatial resolutions. The interpolation is formulated into a regression problem, and a spatial Gaussian Process is proposed to solve the regression problem. The framework is applied to the estimation of $PM_{2.5}$ concentrations across California.

Above works attempt to predict and monitor the air quality from a variety of data sources, including the weather, traffic flow, road networks, physical sensors, social media, etc. But some kinds of these data are not easily obtained. For a practical application, it is important to tradeoff among inference accuracy, conciseness, efficiency, and economy. On the other hand, these works exploit some traditional machine learning and data mining techniques, which rely on sophisticated models and well-designed features, to model the correlation among a variety of data sources. There is still room to promote inference accuracy.

2.3 Outdoor-image Based Estimation

Airborne particulate matter brought by the air pollution is the primary cause for visibility degradation in urban metropolitan areas. Towards this end, several works try to estimate air quality level through analyzing outdoor image's visibility or haze level. For example, the authors of [16] employed the state-of-the-art computer vision techniques to estimate haze level (clear, light, or heavy) via photos acquired from online social media. Moreover, the authors [20] designed a mobile APP, AirTick, which leverages image analytics and deep learning techniques to estimate the Pollutant Standards Index (PSI). They extract the haziness component from the images captured by the users and pass the component to the deep neural network for air quality estimation.

In our prior works [30, 31], we have presented an approach that directly inferences $PM_{2.5}$ level via a single image. We extracted several image features such as dark channel, medium transmission, sky color, power spectrum slope, contrast, and saturation. To effectively fuse these heterogeneous and complementary features, we utilized multikernel learning to learn an adaptive classifier based on multiple kernels. The authors [28] exploited a convolutional neural network to estimate air quality ($PM_{2.5}$ and PM_{10} level) based on photos. They designed a negative log-log ordinal classifier to fit the ordinal output well and a modified activation function for air pollution level estimation.

Overall, these works have shown the promise of image-based approaches to estimate and monitor air pollution. But estimating the $PM_{2.5}$ value even level accurately via images is challenging. Because it is difficult to build a precise model to describe the inner relationship between $PM_{2.5}$ and image pixels. Abundant outdoor images with correct label are needed for training the model. However, the sizes of image datasets utilized in existing works are relatively small. Moreover, some works such as [16] and [28] exploited one site's data or the average data to label images from the whole city, that would cause many wrong labels. On the other hand, it is also necessary to combine the image based models and some other data based model to further improve accuracy.

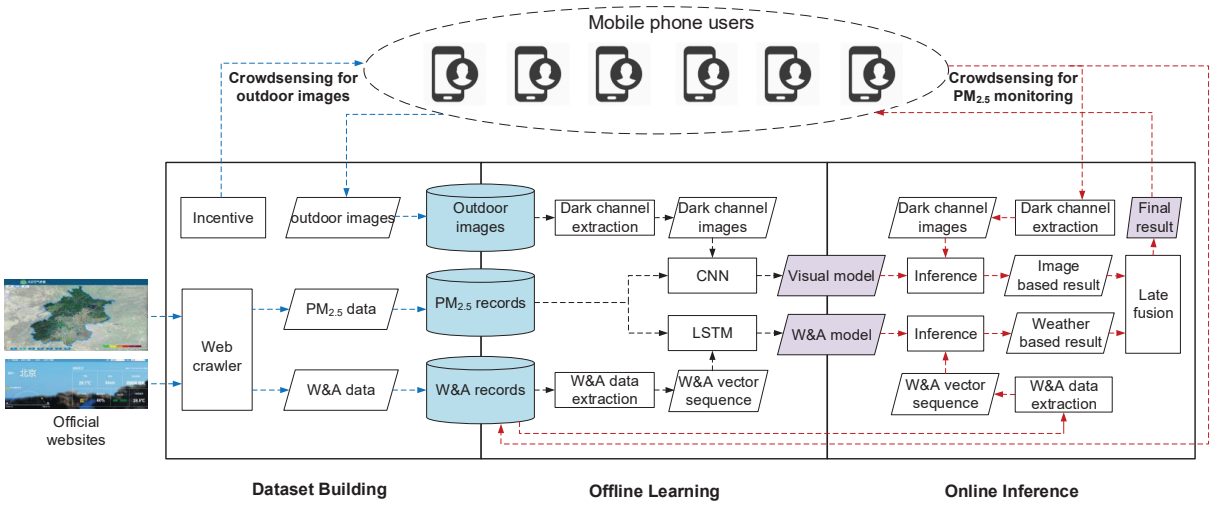

Fig. 3. Framework of the Third-Eye system.

Different from the above related works, we estimate the $PM_{2.5}$ with outdoor-images and temporally-related weather/air-pollutant data. The proposed framework provides a complete solution including dataset generation, offline learning, and online inference. Our work implement combination of accuracy, low cost, portability, and convenience into a single design.

3 SYSTEM OVERVIEW

In this paper, we utilize the outdoor-images taken by mobilephones, weather data, and air-pollutant data to inference $PM_{2.5}$ level and value via machine learning technologies. Thus, as shown in Fig. 3, the framework of our system consists of three major parts: *dataset generation*, *offline learning*, and *online inference*.

3.1 Dataset Generation

In order to comprehensively investigate the air quality monitoring problem, a sufficient dataset, which contains large-scale systemic data collected from expansive location and long period, is necessary. To built such datasets containing outdoor-images, weather and air-pollutant (W&A in short) records, and $PM_{2.5}$ reords, we explore two ways as follows:

- **Crowdsensing for outdoor-images**. The system gives mobilephone users around monitoring sites an incentive to take outdoor-images and send them to the outdoor-image dataset. The system also save the photo-op and place information (which monitoring site the mobilephone user is around) into the outdoor-image dataset.
- **Crawling for W&A and $PM_{2.5}$ data**. The system deploys web crawlers to obtain W&A data and $PM_{2.5}$ data which are generated by weather/air-quality monitoring sites and released by the official websites per hour. We exploit 6 categories of weather data and 4 categories of air-pollution data. For each W&A and $PM_{2.5}$ record, the system also saves the time and space (site ID) information.

Because the $PM_{2.5}$ data generated by monitoring sites is accurate enough to be regarded as the ground truth. Then, for an image sample or W&A sample, it is easy to find the corresponding label, i.e., $PM_{2.5}$ ground truth, via the saved spatio-temporal meta data. See Section 4 for details.

3.2 Offline Training

In this part, the system first preprocesses the collected raw data before training the models. For the outdoor-images, we transform the raw RGB images into the dark channel images which is based on the *dark channel prior*: most local patches in haze-free outdoor images contain some pixels which have very low intensities in at least one color channel [14]. Compared with RGB image, the dark channel image directly reflects the haze level. That means it is more suitable for training the $PM_{2.5}$ inference model. The W&A data is temporally-related, i.e., the value varies with time. Considering that the current $PM_{2.5}$ may be affected by the weather and air-pollution condition several hours ago, we use 48 hours' W&A data (include the current hour and prior 47 hours) to construct a vector sequence. Then, the dark channel images and W&A vector sequence are automatically labeled by querying the $PM_{2.5}$ ground truth dataset. Because of the different characters, our system exploits two deep learning models to train the outdoor-images and W&A data, respectively.

- **Convolutional Neural Network (CNN) for outdoor-images**. As demonstrated as an effective model to automatically learn the visual features and understand image content, CNN attracts growing interests in many computer vision and machine learning tasks. In our system, we train an end-to-end CNN network with dark channel prior to inference the $PM_{2.5}$. Compared with the manually designed features, the features learned by CNN are more robust and effective. Moreover, the dark channel image can remove the most noisy information while keeping the major $PM_{2.5}$ characters, which can help deep neural network quickly capture the discriminative visual information in $PM_{2.5}$ monitoring. Detailed in Section 5.
- **Long short-term memory (LSTM) network for W&A data**. Different from images, the W&A data is a type of sequence data. For the sequence data forest problem, i.e., the W&A based $PM_{2.5}$ inference, it is hard to determine the referred length of the historical sequence to mine the common patterns. Recently, the LSTM network is widely used to explore the dependency and continuity from the sequential data. Due to the hidden layer, LSTM can selectively learn temporal pattern from historical sequence. Therefore, we simply choose a long enough historical W&A data, i.e., 48 hours, as the input. Then the LSTM Network is trained to automatically extract an expressive $PM_{2.5}$ changing information from the long W&A sequence data. Detailed in Section 6.

Then, the offline training generates two types of models: outdoor-images based regression/classification models (visual models for short) and W&A data based regression/classification models (W&A models for short).

3.3 Online Inference

We provide mobilephone users a free APP with friendly interface. When a user takes an outdoor-image using this APP, the image and corresponding time and location information are sent back to the backend server. Then, the system generates the dark channel image and queries W&A data of the latest 48 hours in user's location. After that, the system respectively feeds the dark channel image and W&A vector sequence into the CNN based image model and the LSTM based W&A model, and inferences two results of $PM_{2.5}$ level or value. According to the evaluation, the visual and meteorological models play different roles in different situations. For most of the time, the meteorological model is stable and accurate.

Level	$PM_{2.5}$ Value
0	0-50
1	51-100
2	101-150
3	151-200
4	201-300
5	>300

Fig. 4. Outdoor images dataset. The total number is 31,601 and the numbers of images with level 0-5 are 10,613, 5,521, 4,036, 2,497, 5,643, and 3,291, respectively.

However, only using the meteorological model cannot well estimate the suddenly changed $PM_{2.5}$ value. To holistically exploit the complementary nature of visual and meteorological information for more robust $PM_{2.5}$ value estimation, we choose the average late fusion strategy (i.e., $w = 0.5$) to combine the visual model M_v and meteorological model M_m results as:

$$F = w \times M_v + (1 - w) \times M_m. \tag{1}$$

By calculating the weighted sum of the two results, the system generates the final result and returns it to the user. In user data based evaluation, we test the system performance with different fusion weights. See Section 7 for details.

4 DATASETS GENERATION

As mentioned above, we exploit two ways, crowdsensing and web crawling, to generate three datasets of outdoor-images, W&A data, and $PM_{2.5}$ in Beijing. This section presents the details of the three datasets and the two generation ways, especially for outdoor-image crowdsensing.

4.1 Crowdsensing Based Generation of Outdoor-Image Dataset

In the field of machine learning, collecting mass high-quality samples is very critical but challenging. Because it generally needs amount labor force with high cost. Some researchers start to exploit the crowdsourcing mode to collect and label training samples. ImageNet is a successful example [7]. In this paper, we propose a crowdsensing based solution, which also follows the basic idea of crowdsourcing, to collect and automatically label sensory data in the city.

We recruit some mobile users, whose daily locations are around a monitoring site, to take the outdoor-images. Because the images are taken around the sites, it is easy to obtain the pairs of outdoor-image and $PM_{2.5}$ ground truth. In order to guarantee the sample quality, we require that: 1) the images should be taken within 1 kilometer of a site; and 2) the top $1/3 - 1/2$ area of the captured image is sky. The first rule is based on the fact that the change of $PM_{2.5}$ in a relatively small range is little. Thus, we assume that the places within 1-km radius of a monitoring site have the same $PM_{2.5}$ value (ground truth). To demonstrate this assumption is reasonable, we analyze the 15 months' $PM_{2.5}$ data from two adjacent sites, whose distance is $1.5km$. The average difference of their $PM_{2.5}$ value is only 9.67 $\mu g/m^3$. The second rule is used to avoid indoor or close shot which makes the dark channel work poorly. In order

Table 1. Incentive strategies

Strategy	**Description**
Linear Reward Strategy	The value of each task equals 0.2 RMB. The reward is proportional to the number of tasks participant has accomplished.
Competitive Strategy	We rank participants via the number of completed tasks every day, and choose the top-5 participants to pay 30, 15, 8, 4 and 3 RMB, respectively.
Red Envelope Strategy	When a participant completes a task, he/she will received a red envelope with a random value as the reward. The average value of red envelopes is 0.2 RMB.

Table 2. The order of incentive strategies used in the three universities.

	1-2 week	3-4 week	5-6 week
BUPT	Linear Reward Strategy	Red Envelope Strategy	Competitive Strategy
BIT	Competitive Strategy	Linear Reward Strategy	Red Envelope Strategy
BJU	Red Envelope Strategy	Linear Reward Strategy	Competitive Strategy

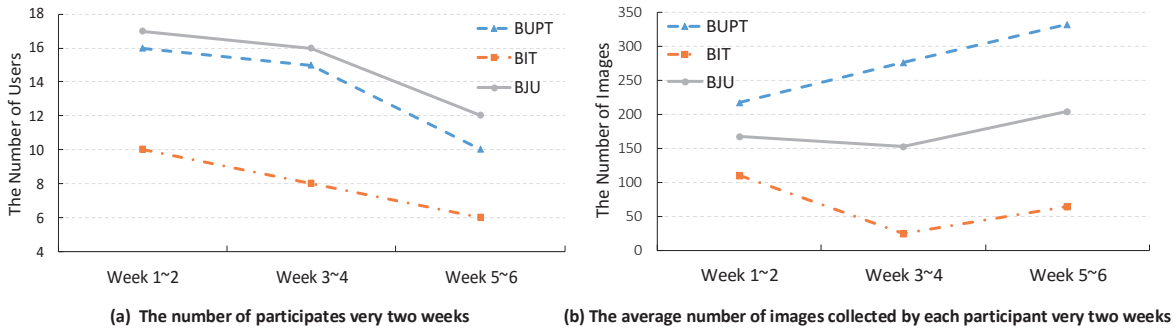

Fig. 5. Comparison of linear reward strategy, competitive strategy, and red envelope strategy.

to reduce the communication and calculation cost, the qualified image is resized as 256×256, and then sent to the outdoor-image dataset. Some examples of the collected images are shown in Fig. 4. Referring to the AQI standards, we classified these images into six categories according to their real $PM_{2.5}$ value.

At first, some students in our lab were willing to be the volunteers. But they lost their passion soon. Therefore, *how to design a proper incentive strategy to attract participants and keep them active* is a key problem for crowdsensing outdoor-images. Incentive is a well-studied problem in the fields of crowdsourcing [26] and crowdsensing [29]. However, many existing incentive strategies are designed for independent tasks. But our system cares about not only the number of completed tasks (taking a out-door image can be regarded as a task) but also the temporal-spatial distribution of samples. That implies that the dataset should include images taken at different times and places. Moreover, many existing works about incentive focus on ideal models based theoretical analysis, thus they cannot be utilized in real application directly.

Fig. 6. Distribution of the 8 monitoring sites covered by the outdoor-image dataset.

By following three classical incentive types, we design three incentive strategies, listed in Table 1, and compare them according to an empirical research of 6 weeks. To make an objective comparison, we recruit some students in three universities: Beijing University of Posts and Telecommunications (BUPT), Beijing Jiaotong University (BJU), and Beijing Institute of Technology in Liangxiang (BIT). The three universities are all nearby a monitoring site (L1, L2, and L3 in Fig. 6). In each university, we change the incentive strategy every two weeks. The detailed schedule is listed in Table 2.[2] Under the total budget of 60 RMB per day for one university, the expected number of images is 300. In order to distribute collected images over the whole day, we release 30 tasks every hour from 9:00 am to 6:00 pm. There are 75 students involved in our experiment. The statistical results of the participant number and average number collected by each participant are illustrated as Figs. 5 (a) and (b), respectively. From the results, we observe that: 1) no matter the order of incentive strategies, the number of participants gradually reduces during the long-term crowdsensing application; 2) from the perspective of average number of image collected by each participant, the competitive strategy is the best one.

We finally recruit more than 200 participants in total to take the outdoor images and build up a large-scale dataset. Overall, the dataset has the following featured properties.

Scale. The outdoor image dataset consists of 31,601 images captured by more than 200 participants from May 2015 to April 2016. These images are captured around 8 monitoring stations and 735 km^2 in the Beijing City (see Fig. 6), which makes the dataset scalable enough for large-scale air quality inference and other related researches. According to our knowledge, our dataset is one of the most comprehensive $PM_{2.5}$ dataset in three aspects: 1) the large image scale–31,601 real-world images captured by 200 people; 2) the long time span–one whole year data; and 3) the massive multisource information–image, time, location, device type, and W&A.

[2]Each participant installs an APP developed by our group for taking/uploading images and recording the earnings. This App also pushes the detailed rules of the incentive strategies to participants beforehand, and notifies them of the change of incentive strategy at each stage.

Accuracy. To get the accurate $PM_{2.5}$ ground truth value, we require the participants should be in the 1-km radius area from the monitoring stations. The distance control is implemented through the GPS positioning of mobilephone. Moreover, the image quality is also controlled by our staffs to ensure its quality and meet our standards.
Diversity. The images are captured in real-world unconstrained scene and tagged with a variety of attributes including $PM_{2.5}$, captured time, location, weather condition, and settings of mobile device. Moreover, the outdoor-image dataset is collected under a wide variety of air pollution condition, seasons, weather and illumination conditions with 73 different types of mobile phones. So complicated models can be learnt and evaluated for $PM_{2.5}$ inference.

4.2 Web Crawling Based Generation of W&A Dataset and $PM_{2.5}$ Dataset

In this paper, we exploit 6 categories of weather data: temperature (TE), pressure (PR), humidity (HU), wind speed (WS), wind direction (WD);[3] and weather condition (WC),[4] and 4 categories of air-pollution data: carbon monoxide (CO), nitrogen dioxide (NO_2), ozone (O_3), and sulfur dioxide (SO_2). These data, generated by meteorological sites and air-quality monitoring sites, can be easily obtained on the Internet.

We implement two web crawlers: one captures the weather data of Beijing's 13 districts which is released by National Meteorological Center;[5] the other one captures the air pollution data from 35 monitoring sites which is released by Beijing Municipal Environmental Monitoring Center.[6] We extract the 35 monitoring sites' $PM_{2.5}$ data from the air pollution data for building the $PM_{2.5}$ dataset, and map the data of CO, NO_2, O_3, and SO_2 into 13 districts. Then, for each district, we generate a W&A record with 10 dimensions per hour. Overall, we collect W&A records and $PM_{2.5}$ records from May 2015. Till now, there are more than 150,000 W&A records in our dataset.

5 THE VISUAL MODEL LEARNING

5.1 Dark Channel Prior

Outdoor-images are usually degraded by the particulate matter, which is one of the main air pollution sources. In the process of transmission, light intensity attenuated because of the particulate matter scattering. Definitely, we are able to infer the air quality via haze degree relying on the atmospheric scattering model and statistics derived from various crowdsensing images. Specifically, the model [14] widely used to describe the formation of a fog/haze image is as follows:

$$I(x) = t(x)J(x) + (1 - t(x))A, \tag{2}$$

where I is the observed image, J denotes the scene radiance, A denotes the atmospheric light, and t denotes the medium transmission describing the portion of the light that is not scattered and reaches the camera. When the atmosphere is homogenous, the medium transmission t can be expressed as haze degree:

$$t(x) = e^{-\beta d(x)}, \tag{3}$$

where β is the scattering coefficient of the atmosphere and d is the scene depth. This equation indicates that the scene radiance is attenuated exponentially with the depth. Based on this model, significant progress has been made in haze removal from a single image.

[3]The values of wind direction include east, west, south, north, unstable, southeast, northeast, southwest, and northwest.
[4]The values of weather condition include sunny, cloudy, overcast, rainy, sprinkle, moderate rain, heaver rain, rain storm, thunder storm, freezing rain, snowy light snow, moderate snow, foggy, sand storm, and dusty.
[5]http://www.nmc.cn/publish/forecast/ABJ/beijing.html
[6]http://zx.bjmemc.com.cn/getAqiList.shtml

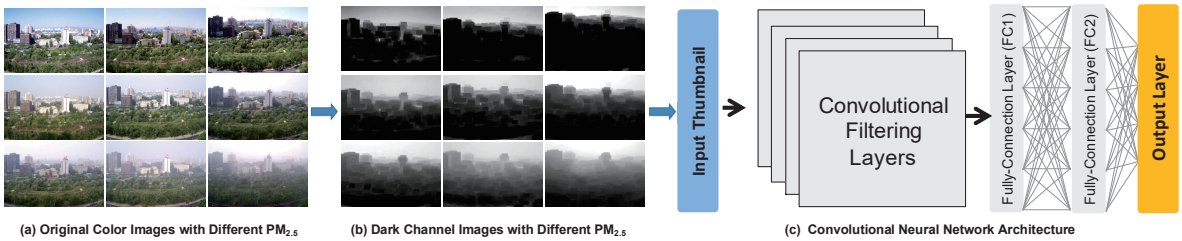

Fig. 7. The framework of Dark Channel Prior based CNN.

The dark channel prior has been well studied in the field of single image haze removal. The authors of [14] found that, in most of the non-sky patches, at least one color channel has some pixels with very low intensity and close to zero, called dark channel prior. Equivalently, the minimum intensity in such a patch is close to zero. The low intensity in the dark channel is mainly due to shadows, colorful objects, and dark surfaces in the images. Formally, for an arbitrary image J, its dark channel J^{dark} is given by

$$J^{dark}(x) = \min_{y \in \Omega(x)} (\min_{c \in \{r,g,b\}} J^c(y)), \tag{4}$$

where J^c is a color channel of J and $\Omega(x)$ is a local patch centered at x. Using the concept of a dark channel, the observation says that if J is an outdoor haze-free image, the intensity of J's dark channel is low and tends to be zero:

$$J^{dark} \to 0. \tag{5}$$

However, due to the additive illumination, a hazy image is brighter than its haze-free version where the transmission t is low. So, the dark channel of a hazy image will have higher intensity in regions with denser haze. We can estimated the medium transmission by

$$\widetilde{t}(x) \quad = \quad 1 - \min_{c}(\min_{y \in \Omega(x)} (\frac{J^c(y)}{A^c})). \tag{6}$$

Fig. 7 shows several ourdoor-images and corresponding dark channels. From these examples, we can find that the $PM_{2.5}$ degree is directly reflected on the dark channel images. Therefore, we try to develop a dark channel based CNN to automatically extract robust and discriminative features to infer the $PM_{2.5}$ situation.

5.2 Dark Channel Prior Based CNN

As an effective model to understand image content and tackle tasks, CNN attracts growing interests in the fields of computer vision and machine learning [10, 15, 17]. CNN is a biologically-inspired variant of multilayer perceptron, which can imitate the human brain through multiple transformation and abstraction. As connecting the stages of feature extracting and classier training, the CNN is trained end to end from raw pixel values to classifier outputs. Therefore, in our framework, we exploit CNN as our classifiers to estimate the $PM_{2.5}$.

For conventional CNN architecture, the raw images are directly input into the convolutional layers to extract the visual features. Compared with the manually designed features, the features learned by CNN are more robust and effective. However, the CNN requires to learn sufficient features from a mass of training data for all the categories, e.g., millions of images for image classification. On the other hand, for the applications of air quality monitoring, people may capture the images from diverse place, e.g.,

city, mountain, forest, sea, even indoor. Therefore, it is very hard to collect enough data to support the air quality feature learning from the raw images. To solve the challenge, instead of direct using the raw captured images, we input the dark channel image into the CNN to learn sufficient features. The dark channel image can remove the most noisy information while keeping the major maze characters. Therefore, the dark channel image representation, which is robust to the visual content changes, can help deep neural network quickly capture the discriminative visual information in air quality monitoring.

5.3 Implementation

The implementation of our Dark Channel Prior based CNN has three main parts: network architecture, offline network training and online prediction. For the network architecture, we leverage the CNN architecture as discussed in [15] by adapting their publicly released Caffe-BLVC model [7] as its good performance on ImageNet dataset. The original CNN consists of two parts: 1) the input layers, five convolution layers and maxpooling layers, and 2) two fully connection layers and the output layers which produces probabilities over the 1,000 class labels. For the $PM_{2.5}$ classification, we directly change the 1,000 label output to the number of air quality categories (i.e., 6). Differently, for the $PM_{2.5}$ regression task, we change the classification loss layer to the regression loss layer.

In the training state, our training algorithm adopts the mini-batch stochastic gradient descent for optimizing the objective function. After transforming the original RGB images into the dark channel images, the training data is divided into mini-batches. Training errors are calculated upon each mini-batch in the loss layer and backward propagated to the lower layers. The network weights are updated simultaneously. We set learning rate policy to "step". We initialize the learning rate to 10^{-2} and gamma to 10^{-1}. Momentum, weight decay and stepsize are set to 9×10^{-1}, 5×10^{-4} and 4.5×10^{5} respectively.

After training, the well optimized models can be used for online classification and regression. Specifically, we first utilize the pre-trained model to initialize the network. Then we send the target image into the CNNs, and compute the feed-forward network based on the matrix multiplication for one time to extract discriminative features. Finally, we are able to obtain the probabilities of 6 air quality categories and regression value through the corresponding loss functions.

5.4 Evaluations of the Visual Model

In the experiments, we evaluate the proposed Dark Channel Prior based CNN model on the collected 31,601 images in crowdsensing based dataset. The evaluations are given in three different settings: 1) random division, 2) temporal division, and 3) spatial division. Firstly, the random division randomly divides all the images captured at 8 different monitoring sites from May 2015 to April 2016 to training, validation and test dataset. The training set contains 26,680 images, test set contains 1,121 images, and the validation contains 4,921 images. This is a baseline division in which the images captured in near locations and time are randomly divided. It means that for each test image, the learned model may see the similar images in the training set. Next, temporal division divides the training, validation and test images according to different shooting time. The goal of temporal division is to evaluate whether the model trained on the historical data can accurately estimate the real-time $PM_{2.5}$ value. The images captured in the front three weeks of each month are selected as the training data, the rest images are set as the testing data. As we have 12 month data, it is a 12-fold validation. We divided the data in each month as we online update our model with the past three weeks $PM_{2.5}$ history in the real-world implementation. Finally, in the location division, we choose the images from the seven different places as training date to train the visual model. Then the model is exploited to estimate PM2.5 value in the rest

[7] "Caffe Model Zoo," http://caffe.berkeleyvision.org/model_zoo.html

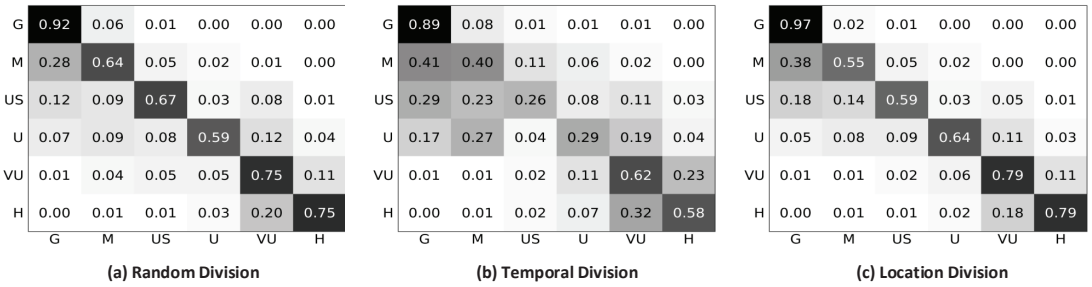

Fig. 8. The confusion matrix of visual model evaluation in different divisions.

one location. The goal of spatial division is to evaluate the expansibility of the proposed model—whether the model can perform well in the place where there is no training data. As we described before, the images from different places have significant diverse visual content. The diversity is a great challenge for visual information based $PM_{2.5}$ estimation. We alternately set each place as testing and totally do 8 groups of experiments. So it is a 8-fold validation.

The experimental results of random division and temporal division are shown in Fig. 8 and Table 3. The Fig. 8 shows the confusion matrix of different division. The rows of the matrix are the real $PM_{2.5}$ categories. The columns are the predicted $PM_{2.5}$ categories. We can see that in the random division, the proposed visual model can well discriminate the 6 different categories. In the temporal division, the performances on the middle categories are worse than the two ends. The comparative results in Table 3 show that the proposed Dark Channel Prior based CNN is better than the color images based one on whether the classification accuracy or regression error. It demonstrates that the dark channel prior can help CNN better detect the $PM_{2.5}$ pollution and be more robust to the visual content change. Specially, the results of temporal division shows that the model trained on the historical data can be exploited to estimate the real-time $PM_{2.5}$ value.

For the spatial division, we alternately set each place as testing and totally do 8 groups of experiments. The average classification accuracy and regression error is shown in Fig. 9. The results demonstrate that although the model do not see the data from that place, it can still well estimate its $PM_{2.5}$ value. For example, from Fig. 6, we can find that L2 is the farthest place from each other. Its classification accuracy (73.54%) is still higher than the average accuracy (72.04%). The experimental results of spatial division demonstrate that the usable range of the proposed system is not limited to the proposed eight locations with training data.

6 THE W&A MODEL LEARNING

6.1 W&A Data Extraction

Through dark channel prior based CNN, we can extract a discriminative high-level visual information to estimate the $PM_{2.5}$ value. However, in the air quality monitoring problem, as we discussed before, the visual information still has poor robustness on wide varieties of captured images with different viewpoints, illusion, and background. Besides, because of 1) the great semantic gap between $PM_{2.5}$ and dark channel visual information, and 2) the diversity visual content of different training images as shown in Fig. 4, it is hard to learn a general mapping model from limited image data. On the other hand, W&A data is widely

Table 3. The classification accuracy and regression error of visual model evaluation in different divisions.

Division	Methods	Classification Accuracy	Regression Error
Random division	Color Image based CNN	74.65%	24.89
	Dark Channel based CNN	77.92%	22.89
Temporal division	Color Image based CNN	59.39%	39.74
	Dark Channel based CNN	62.05%	37.21
Spatial division	Color Channel based CNN	69.84%	29.86
	Dark Channel based CNN	72.04%	27.37

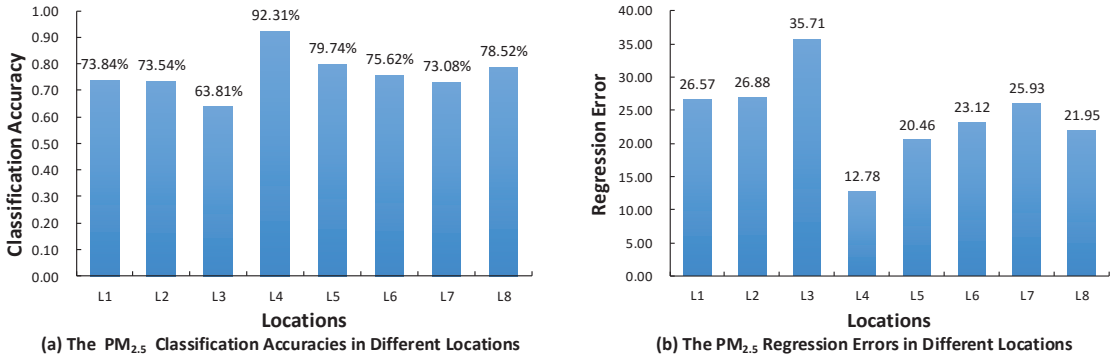

Fig. 9. The results of the spatial division based visual model evaluations.

used to forecast local air quality [4]. Because the urban air quality varies by different weather conditions. For example, gale wind always help to reduce the concentration of $PM_{2.5}$. Therefore, to achieve more accurate and robust Air Quality Monitoring performance, we extract W&A vectors to supplement the visual information.

The W&A data contains two meaningful information, spatial-based local weather condition and temporal-based weather changing situation. For the spatial information, taking Beijing City as a case study, we can obtain the W&A information through weather forecast on the scale of districts in every one hour. Then, the extracted W&A features will reflect the current air quality condition in the specific regions. For the temporal one, we observe that the historical weather condition has great influence on the posterior air quality index. As shown in Section 3.1, we collect 10 types of fine-grained W&A data, consisting of weather condition, temperature, pressure, humidity, wind speed and direction, concentrations of CO, NO_2, O_3 and SO_2 from Beijing Municipal Environmental Monitoring Center and National Meteorological Center. Moreover, from the historical $PM_{2.5}$ data, we observed the phenomenon that the value of the $PM_{2.5}$ in each day is hard to be the same, but the variation mostly follows a similar changing pattern, because of the traffic flow or human mobility in rush hour. So we bring extra time stamp feature, which represents the relevant information instead of the raw traffic or human mobility information, for avoiding introducing additional semantic gap. Finally, we can obtain a 11-dimensional feature vector to

represent W&A information at one specific time point as:

$$W\&A\ Vector =< WC, TE, PR, HU, WS, WD, CO, NO_2, O_3, SO_2, Time > .$$

By integrating spatial and temporal W&A data, our framework has great potentials to achieve accurate and robust air quality analysis.

6.2 W&A Based LSTM Network

For covering the semantic gap between the $PM_{2.5}$ information and visual information, we attempt to build another homogenous mapping model from readily available W&A data to $PM_{2.5}$ data. However, we discovered that the directly mapping model from available W&A data to exact $PM_{2.5}$ still cannot handle the dramatically $PM_{2.5}$ changing situation or singular value point. Therefore, we wish to distill the changing pattern of the historical W&A information to help predicting the current $PM_{2.5}$ value. The traditional sequence prediction models, such as Hidden Markov Model and Dynamic Bayesian Network System, require to refer fixed-length history data. However, for $PM_{2.5}$ estimation, it is very hard to determine how long history data is needed in the predictive model. The length is determined according to different weather condition.

Fortunately, Recurrent Neural Network (RNN), a special type of neural network, is exposed of remarkable memory ability in Natural Language Processing (NLP) problems. Indeed, the primary aim of RNN is exploring the dependency and continuity from the sequential data. Due to the hidden layer, RNN can selectively learn temporal information from historical sequence. In the air monitoring problem, although the exact $PM_{2.5}$ value is hard to be predicted by discrete W&A data, the variation of $PM_{2.5}$ still follows a consecutive pattern because of the diffusion of atmosphere, which brings RNN an unmissable opportunity to obtain the W&A temporal information. So in this paper, we adopt the primary idea of RNN to design a temporal framework for extracting an expressive W&A changing information.

To model a long term W&A change pattern from the readily available data, we adopt the typical Long Short-Term Memory Network (LSTM), an effective RNN model, on the 11 (dimensional) $\times$ 48 (hour) readily available W&A data matrix obtained from monitoring station. Different from standard tanh-RNN, the special gate mechanism in LSTM can handle the vanishing gradient problems, and with the help of memory cell, it can memorize or forget the historical W&A information in each timestep. In this paper, we select the 2-layer LSTM architecture with 128 hidden cells as described in [9].

At each timestep t, we input the 11 dimensional W&A feature, like air temperature, pressure, humidity, wide speed and direction, weather condition, the concentrations of CO, NO_2, O_3 and SO_2, and the time stamp feature as x_t. The output feature h_t contains the temporal W&A information we interested. $\mathbf{W}$ are the input weighted matrices, $\mathbf{R}$ are the recurrent weighted matrices, and $\mathbf{b}$ are the bias vectors. The sigma and tanh are nonlinear activation functions, mapping real values to (0,1) and (-1,1). The $\odot$ and $\oplus$ represents the dot product and the sum of two vectors respectively. Given x_t and h_{t-1}, LSTM unit updates for timestep t are:

$$\begin{aligned}
g_t &= \phi(\mathbf{W}_g x_t + \mathbf{U}_g h_{t-1} + \mathbf{b}_g) \\
i_t &= \sigma(\mathbf{W}_i x_t + \mathbf{U}_i h_{t-1} + \mathbf{b}_i) \\
f_t &= \sigma(\mathbf{W}_f x_t + \mathbf{U}_f h_{t-1} + \mathbf{b}_f) \\
c_t &= g_t \odot i_t + c_{t-1} \odot f_t \\
o_t &= \sigma(\mathbf{W}_o x_t + \mathbf{U}_o h_{t-1} + \mathbf{b}_o) \\
h_t &= \phi(c_t) \odot o_t
\end{aligned}$$

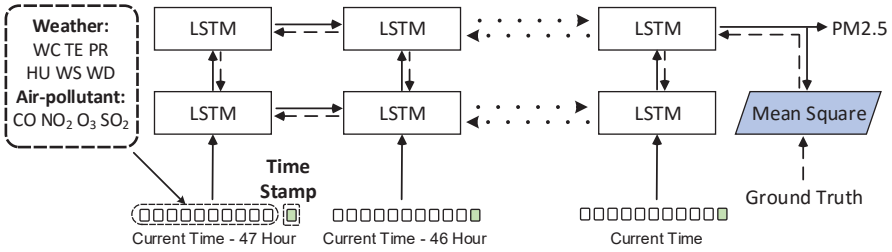

Fig. 10. The framework of W&A based LSTM model.

As shown in Fig. 10, our framework of the W&A based LSTM model adopts a successive estimation strategy. In order to estimate the current $PM_{2.5}$, a 47-hour historical meteorological sequence data and the current meteorological data are required. For training the LSTM temporal estimation model, we split the whole meteorological data into several 48-hour continuous sequence according to their time stamp. The training data is consisted of 10 dimensional feature, which contains the available meteorological data like air temperature, pressure, humidity, wide speed and direction, the concentrations of CO, NO_2, O_3, SO_2, and the weather code transformed from raw weather condition. Then we supplement each 10 dimensional meteorological data with their corresponding time stamp to form the 11 dimensional W&A vector. Therefore, in the training process, we define a 48 time step LSTM model with 128 hidden neurons and feed the 11 dimensional vector in each iteration. Besides, the L2 loss is calculated by Eq. (7) upon each N mini-batch and backward propagated through time.

$$L = \frac{1}{N}\sum_{i} |pred_i - label_i|^2, i \in \{0, 1...N-1\}. \tag{7}$$

For optimizing the stochastic functions, we adopt the Adam algorithm [9] and initialize the learning rate to 0.001, the exponential decay rate for the 1st moment estimates to 0.9, the exponential decay rate for the 2st moment estimates to 0.999 and the epsilon to $1 \times e^{-8}$.

6.3 Evaluations of the W&A Model

In the experiments, we evaluate the proposed W&A features and models on the collected 13 districts' weather data from May 2015 to July 2017. The records in the front three weeks of each month are selected as training, and the left records are selected as testing. To evaluate the effects of different W&A features, we divide the W&A features into three different groups: 1) Weather (W): weather condition, temperature, pressure, humidity, wind speed, and wind direction; 2) Air Quality (A): CO, NO_2, O_3, and SO_2; and 3) Time Stamp (T). We compare different combinations of the W&A features.

The confusion matrix of classification results are shown in Fig. 11. The rows of the matrix are the real $PM_{2.5}$ categories. The columns are the predicted $PM_{2.5}$ categories. The average classification accuracies and regression errors of different methods are shown in Table 4. From the results, we can find that more meteorological features are utilized, higher estimation performance is achieved. This demonstrate that all the selected meteorological features are useful to estimate the $PM_{2.5}$. In detail, from the confusion matrix, we can find that if only using the weather information, most of the records are classified into the G and M categories. It means that if only using whether information, it is hard to detect the $PM_{2.5}$ situation. Moreover, after adding the air quantity information, classification accuracy is greatly

Table 4. The comparison of different W&A feature based LSTM models.

Methods	Classification Accuracy	Regression Error
W	62.43%	36.54
A	70.26%	28.50
W+A	72.96%	26.52
W+A+T	75.21%	23.72

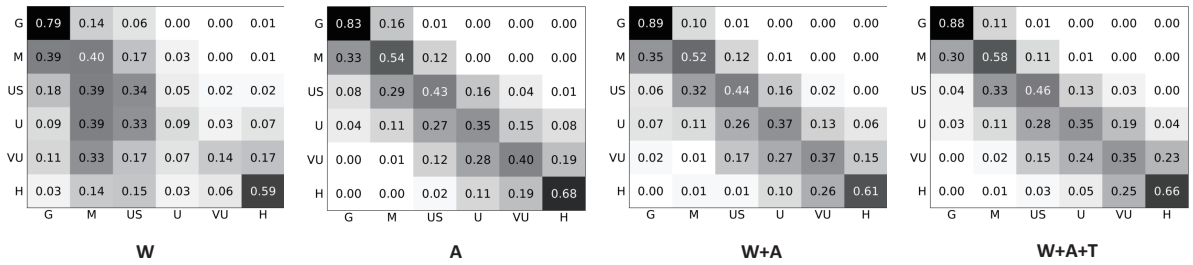

Fig. 11. The confusion matrix of different W&A feature based LSTM models.

improved. The confusion matrix also more obviously shows the improvements. Different from weather information, the false classifications mainly appear in the adjacent categories. Furthermore, the addition of T can further decrease the obviously wrong situation. According to our further observation, the wrong situations mainly appear in the boundary of each categories. The regression errors also demonstrate this conclusion. Finally, the proposed W&A model can achieve 75.21% classification accuracy with only 23.72 regression error.

7 APPLICATION AND EVALUATION

Based on our framework and models, we develop a mobile APP - Third-Eye. This is an analogy that the camera of mobilephone works like the third eye of users. Using "the third eye", users are able to see the real-time $PM_{2.5}$ concentration. We have developed three versions for Andriod, iOS, and WeChat, respectively. All these versions are downloaded more than 2,000 times. An ideal personal air monitor necessitates the combination of accuracy, low cost, portability, and convenience into a single design. In this section, we show the application of Third-Eye, and demonstrate how Third-Eye offers substantial enhancements over some other commercial $PM_{2.5}$ monitors by simultaneously improving accessibility, portability, and accuracy.

7.1 Interface

As shown in Fig. 12, this APP provides a very concise and friend interaction interface. When a user opens the APP, it automatically launches the rear camera of mobilephone soon. The APP interface (see Fig. 12(b)) guides the user to take the quantified outdoor images. It provides a white box which is a suggested sky area of the image. We need the outdoor-image including a part of sky, because it can avoid indoor or close shot which makes the dark channel work poorly. After pressing the capture button, the image is taken, and then resized as 256×256 pixels. The image is sent to the back-end server which runs

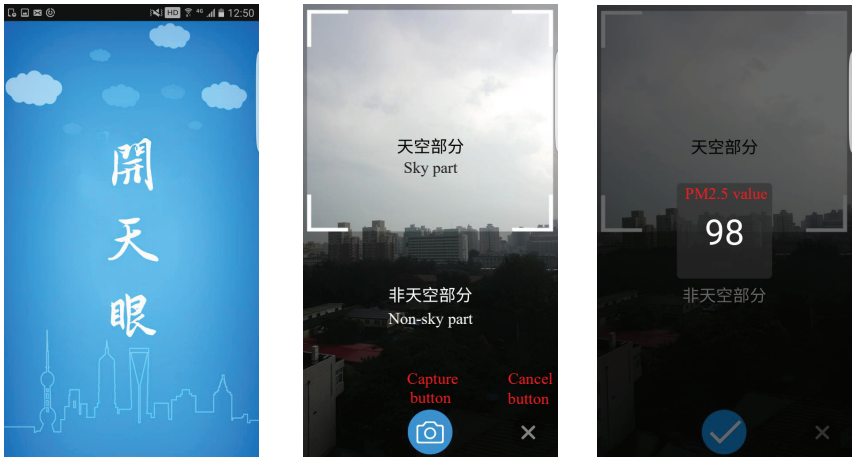

(a) (b) (c)

Fig. 12. Screenshot of Third-eye. (a) The boot screen. The three Chinese characters mean opening the third eye. (b) The interface of capturing outdoor-image. (c) The interface of returning result.

the inference models (regression models based on outdoor-image and W&A data). The server calculates the $PM_{2.5}$ value and returns it to user's mobilephone. Fig. 12(c) illustrates the interface of result display.

7.2 Accuracy

Next, we further evaluate the performance of Third-Eye via user data analysis. The beta version of Third-Eye (for Android) has started running from July 2016. We choose the data generated by users around monitoring sites, and then obtain 1,198 records of user data with $PM_{2.5}$ ground truth from July 2016 to July 2017. We first compare the APP results with the ground truth. As shown in Fig. 13, for most time the difference between APP result and the ground truth is very small. The average error is 17.38 and the classification accuracy is 81.55%.

We further evaluate different fusion weights to investigate the effects of visual and W&A models in the final system. We change the weight w from 0 to 1 with the step of 0.05, and calculate the corresponding regression error and classification accuracy for each value of w. The results are illustrated in Fig. 14. When $w = 0$, i.e., only using W&A model, the regression error and classification accuracy are 22.06 and 78.29%, respectively; when $w = 1$, i.e., only using visual model, the regression error and classification accuracy are 33.81 and 61.52%, respectively. That means the combination of the two models can significantly improve the inference performance. From Fig. 14, we also observe that when w is around 0.5, the relatively low regression error and high classification accuracy are achieved. This result is consistent with the setting of $w = 0.5$.

7.3 Computational Time

To evaluate the computational complexity of the proposed system, we further calculate the processing time of the 1,198 user records. The results are shown in Fig. 15. Because the user scale is not large, the server-side is now executed on the computer with Intel Xeon E5-2620v3 2.4GHz CPU and 16G memory without any GPU devices. From the Fig. 15, we can find that most of the computational time is less than 2 seconds. The average computation time is 1.31 seconds. We also test the system on the graphic

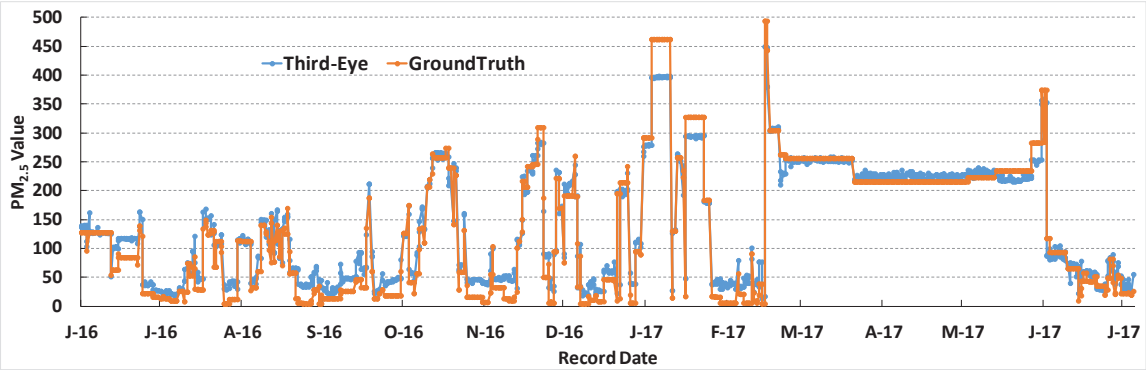

Fig. 13. The real-world $PM_{2.5}$ inference accuracy of the proposed system.

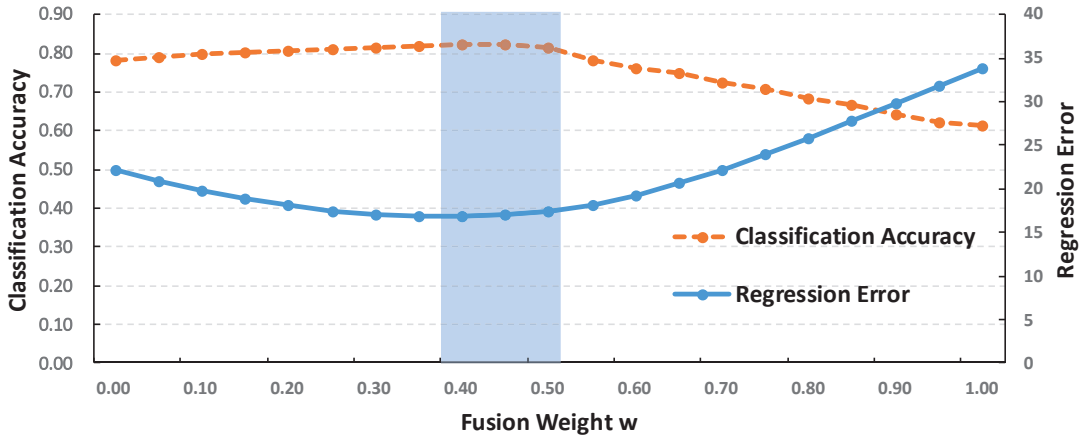

Fig. 14. Fusion results of visual and W&A models with different weights.

workstation with Intel Xeon E5-2660v3 2.6GHz CPU, four NVIDIA K80m GPU cards, 256G memory, and 1T SSD disk. The average computation time is 210ms. We think the computation time can be limited in 100ms after optimizing the code.

7.4 Comparison

First of all, we compare the proposed Third-Eye with the following state-of-the-art air quality monitoring solutions:

- **PAPLE [28]**. PAPLE exploits a CNN to estimate air quality based on photos. They designed a negative log-log ordinal classifier to fit the ordinal output and a modified activation function for air pollution level estimation.

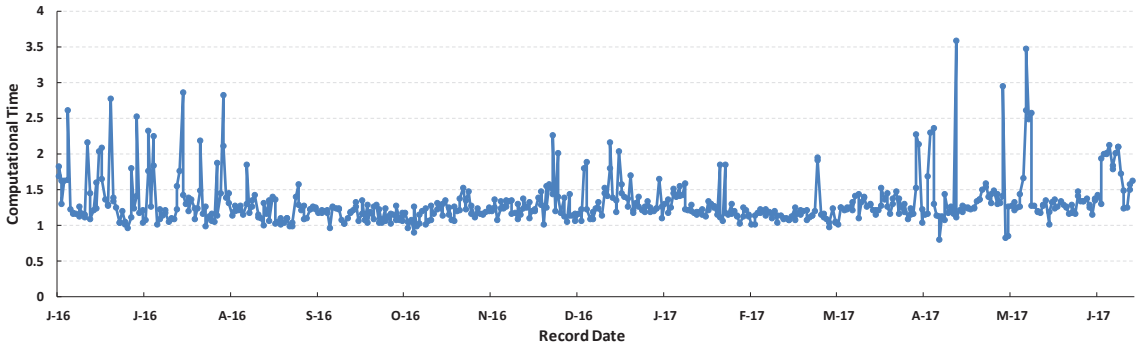

Fig. 15. The real-world computation time for $PM_{2.5}$ inference.

- **AirTick [20]**. AirTick is a mobile APP which leverages image analytics and deep learning techniques to produce accurate estimates of air quality with camera enabled smart mobile device.
- **Scattered Interpolation**. With the $PM_{2.5}$ values from 34 monitoring sites (exclude the ground truth monitoring site), three commonly used scattered interpolation methods, *Linear Interpolation*, *Nearest Neighbor Interpolation*, and *Natural Neighbor Interpolation*, are employed to estimate the $PM_{2.5}$ of the ground truth monitoring site.
- **Dark Channel based CNN**. This is the proposed visual model.
- **W+A+T based LSTM**. This is the proposed W&A model.
- **Third-Eye**. This is the proposed mobilephone-enable system combined the visual model with the W&A model.

The evaluations are performed on the 1,198 records of user data with $PM_{2.5}$ ground truth captured from July 2016 to July 2017. The compared results, i.e., classification accuracy and regression error, are listed in Table 5. From the results, we can find that compared with the state-of-the-art visual information based methods (i.e., PAPLE and AirTick), the proposed dark channel based CNN achieves the better performance. It demonstrate that the proposed dark channel prior can remove the most noisy information while keeping the major maze characters, which leads the CNN to effectively extract the discriminative and robust features for $PM_{2.5}$ estimation. Moreover, compared with the traditional interpolation methods, our W&A model also has much better accuracy. This demonstrates that the proposed W&A model can extract expressive features from long consecutive W&A changing patterns with the LSTM. Finally, compared with all the state-of-the-art solutions, the proposed Third-Eye, which combines the Dark Channel based CNN and W+A+T based LSTM, achieves the best performance.

Moreover, we also compare the performances between Third-Eye and 4 popular commercial $PM_{2.5}$ monitors. We bring these devices to the places nearby a monitoring site (L1 in Fig. 6), and collect more than 6,000 measurements over three months. Compared with the ground truth, we find the $PM_{2.5}$ measurements generated by portable devices are with relatively large errors and low stability. Taking Dylos 1700 for example, it is commonly used in many research works to provide high quality $PM_{2.5}$ data. But its average error is 43.43 in our tests. As shown in Fig. 16, our system achieves the best results with only 17.38 average error. Fig. 16 also lists the price, size, and weight of each device. As the mobilephone become the indispensable tool for each people, our APP is near zero cost. The users do not

Table 5. The comparison between Third-Eye and state-of-the-art air quality monitoring algorithms.

Methods	Classification Accuracy	Regression Error
PAPLE [28]	47.91%	33.79
AirTick [20]	50.33%	–
Linear Interpolation	64.81%	39.80
Nearest Neighbor Interpolation	61.76%	46.79
Natural Neighbor Interpolation	64.72%	39.82
Dark Channel based CNN (Ours)	61.52%	33.81
W+A+T based LSTM (Ours)	78.29%	22.06
Third-Eye (Ours)	**81.55%**	**17.38**

Device	GEETEE	LVCHI	Hanvon	Dylos	Third-Eye
Appearance					
Price	$90	$75	$150	$425	Free
Size (mm)	109 x 71 x 42	144 x 86 x 60	119 x 62 x 23	178 x 114 x 76	--
Weight	250g	460g	160g	544g	--
Error	**28.69**	**77.66**	**28.55**	**43.43**	**17.38**

Fig. 16. The comparison between Third-Eye and four commercial $PM_{2.5}$ monitors.

need to specially take a unnecessary portable devices and can get the real-time $PM_{2.5}$ data at any place in Beijing.

7.5 Limitations

Compared with portable $PM_{2.5}$ monitors, Third-Eye shows its advantages in terms of accuracy, portability, and price. But there are also three main limitations of our APP:

- In the phase of model training, we use the images taken within 1 kilometer of sites as the training samples. This implies that the places within 1-km radius of monitoring site have the same $PM_{2.5}$ value (ground truth). Moreover, the $PM_{2.5}$ ground truth and W&A data are generated per hour, i.e., these kinds of data are assumed to be steady during a hour. These hypotheses will affect the spatial/temporal resolution of our APP.
- Our developed models are not suitable for indoor environment. Because for most indoor images the distance between the shot scene and the camera is not far, that causes the low discrimination of dark channel (see Eq. (3)). Furthermore, compared to the outdoor environment, the weather conditions have less effect on indoor $PM_{2.5}$. That means the W&A model also does not work well.
- Our outdoor image based model cannot work at night, and only W&A model works for night use. That means compared with the daytime, the performance of Third-Eye declines at night. But our APP also can achieve 75.12% classification accuracy and 23.72 regression error for night use (see the part of W&A model evaluation in Section 6.3).

8 CONCLUSION

In this paper, we propose a mobilephone-enabled crowdsensing system named Third-Eye to estimate the $PM_{2.5}$. First of all, we recruit more than 200 participants with various crowdsensing incentive strategies to collect one of the most comprehensive $PM_{2.5}$ estimation dataset, which includes 31,601 labeled outdoor images, one whole year time span, and the 150,000 W&A records. Moreover, with these valuable data, we holistically train two different end-to-end models: the dark channel prior based CNN model and the W&A based LSTM model. In the first model, the dark channel prior is computed to remove the most noisy information while keeping the major maze characters, and the CNN is learnt to estimate the $PM_{2.5}$ from the dark channel image. Meanwhile, the W&A based LSTM model exploits the recurrent neural network to extract the $PM_{2.5}$ changing pattern from the historical meteorology sequence information. Finally, the two complementary models are combined by the late fusion strategy. To evaluate the proposed system, we release three applications for Andriod, iOS, and WeChat users, respectively. Through one more year real-world evaluation based on crowdsensing incentive strategies, more than 2,000 users in Beijing downloaded our system and supply the actual usage data. The user data analysis sufficiently verify that our APP significantly outperforms 5 state-of-the-art methods and 4 popular portable devices.

Furthermore, although in this paper we only test the Third-Eye in Beijing, the evaluations demonstrate that the proposed system has the adequate expansibility to be used in other cites. In the future, we will try to develop its global version to help more users conventionally monitor the air quality and protect their health.

ACKNOWLEDGMENTS

This work is partially supported by National Key R&D Program of China Grant (No.2017YFB1003000), and National Natural Science Foundation of China Grant (No.61332005, No.61720106007, and No.61632008).

REFERENCES

[1] AR Al-Ali, Imran Zualkernan, and Fadi Aloul. 2010. A mobile GPRS-sensors array for air pollution monitoring. *IEEE Sensors Journal* 10, 10 (2010), 1666–1671.

[2] Paul M. Aoki, R. J. Honicky, Alan M. Mainwaring, Chris Myers, Eric Paulos, Sushmita Subramanian, and Allison Woodruff. 2009. A vehicle for research: using street sweepers to explore the landscape of environmental community action. In *Proceedings of the 27th International Conference on Human Factors in Computing Systems, Boston, MA, USA*. 375–384.

[3] Elena Boldo, Sylvia Medina, Alain Le Tertre, Fintan Hurley, Hans-Guido Mücke, Ferrán Ballester, Inmaculada Aguilera, and others. 2006. Apheis: Health impact assessment of long-term exposure to PM2. 5 in 23 European cities. *European journal of epidemiology* 21, 6 (2006), 449–458.

[4] Jiaoyan Chen, Huajun Chen, Jeff Z. Pan, Ming Wu, Ningyu Zhang, and Guozhou Zheng. 2013. When big data meets big smog: a big spatio-temporal data framework for China severe smog analysis. In *Proceedings of the 2nd ACM SIGSPATIAL International Workshop on Analytics for Big Geospatial Data, Orlando, FL, USA*. 13–22.

[5] Jiaoyan Chen, Huajun Chen, Guozhou Zheng, Jeff Z. Pan, Honghan Wu, and Ningyu Zhang. 2014. Big smog meets web science: smog disaster analysis based on social media and device data on the web. In *23rd International World Wide Web Conference, Seoul, Republic of Korea*. 505–510.

[6] Yun Cheng, Xiucheng Li, Zhijun Li, Shouxu Jiang, Yilong Li, Ji Jia, and Xiaofan Jiang. 2014. AirCloud: a cloud-based air-quality monitoring system for everyone. In *Proceedings of the 12th ACM Conference on Embedded Network Sensor Systems, Memphis, Tennessee, USA*. 251–265.

[7] Jia Deng, Wei Dong, Richard Socher, Li-Jia Li, Kai Li, and Li Fei-Fei. 2009. Imagenet: A large-scale hierarchical image database. In *IEEE Conference on Computer Vision and Pattern Recognition*. IEEE, 248–255.

[8] Srinivas Devarakonda, Parveen Sevusu, Hongzhang Liu, Ruilin Liu, Liviu Iftode, and Badri Nath. 2013. Real-time air quality monitoring through mobile sensing in metropolitan areas. In *Proceedings of the 2nd ACM SIGKDD International Workshop on Urban Computing, Chicago, Illinois, USA*. 15:1–15:8.

[9] Jeff Donahue, Lisa Anne Hendricks, Marcus Rohrbach, Subhashini Venugopalan, Sergio Guadarrama, Kate Saenko,

and Trevor Darrell. 2017. Long-Term Recurrent Convolutional Networks for Visual Recognition and Description. *IEEE Trans. Pattern Anal. Mach. Intell.* 39, 4 (2017), 677–691.

[10] Chuang Gan, Naiyan Wang, Yi Yang, Dit-Yan Yeung, and Alexander G. Hauptmann. 2015. DevNet: A Deep Event Network for multimedia event detection and evidence recounting. In *IEEE Conference on Computer Vision and Pattern Recognition*. 2568–2577.

[11] Raghu K. Ganti, Fan Ye, and Hui Lei. 2011. Mobile crowdsensing: current state and future challenges. *IEEE Communications Magazine* 49, 11 (2011), 32–39.

[12] Yi Gao, Wei Dong, Kai Guo, Xue Liu, Yuan Chen, Xiaojin Liu, Jiajun Bu, and Chun Chen. 2016. Mosaic: A low-cost mobile sensing system for urban air quality monitoring. In *35th Annual IEEE International Conference on Computer Communications, San Francisco, CA, USA*. 1–9.

[13] Bin Guo, Zhu Wang, Zhiwen Yu, Yu Wang, Neil Y. Yen, Runhe Huang, and Xingshe Zhou. 2015. Mobile Crowd Sensing and Computing: The Review of an Emerging Human-Powered Sensing Paradigm. *ACM Comput. Surv.* 48, 1 (2015), 7:1–7:31.

[14] Kaiming He, Jian Sun, and Xiaoou Tang. 2011. Single Image Haze Removal Using Dark Channel Prior. *IEEE Trans. Pattern Anal. Mach. Intell.* 33, 12 (2011), 2341–2353.

[15] Alex Krizhevsky, Ilya Sutskever, and Geoffrey E. Hinton. 2012. ImageNet Classification with Deep Convolutional Neural Networks. In *26th Annual Conference on Neural Information Processing Systems, Lake Tahoe, Nevada, United States*. 1106–1114.

[16] Yuncheng Li, Jifei Huang, and Jiebo Luo. 2015. Using user generated online photos to estimate and monitor air pollution in major cities. In *Proceedings of the 7th International Conference on Internet Multimedia Computing and Service, Zhangjiajie, Hunan, China*. 79:1–79:5.

[17] Wu Liu, Tao Mei, Yongdong Zhang, Cherry Che, and Jiebo Luo. 2015. Multi-task deep visual-semantic embedding for video thumbnail selection. In *IEEE Conference on Computer Vision and Pattern Recognition, Boston, MA, USA*. 3707–3715.

[18] Huadong Ma, Dong Zhao, and Peiyan Yuan. 2014. Opportunities in mobile crowd sensing. *IEEE Communications Magazine* 52, 8 (2014), 29–35.

[19] XY Ni, H Huang, and WP Du. 2017. Relevance analysis and short-term prediction of PM 2.5 concentrations in Beijing based on multi-source data. *Atmospheric Environment* 150 (2017), 146–161.

[20] Zhengxiang Pan, Han Yu, Chunyan Miao, and Cyril Leung. 2017. Crowdsensing Air Quality with Camera-Enabled Mobile Devices. In *Proceedings of the Thirty-First AAAI Conference on Artificial Intelligence, San Francisco, California, USA*. 4728–4733.

[21] Sameera Poduri, Anoop Nimkar, and Gaurav S Sukhatme. 2010. Visibility monitoring using mobile phones. *Annual Report: Center for Embedded Networked Sensing* (2010), 125–127.

[22] Mette Sørensen, Bahram Daneshvar, Max Hansen, Lars O Dragsted, Ole Hertel, Lisbeth Knudsen, and Steffen Loft. 2003. Personal PM2. 5 exposure and markers of oxidative stress in blood. *Environmental Health Perspectives* 111, 2 (2003), 161.

[23] Mengfan Tang, Xiao Wu, Pranav Agrawal, Siripen Pongpaichet, and Ramesh Jain. 2017. Integration of Diverse Data Sources for Spatial PM2.5 Data Interpolation. *IEEE Trans. Multimedia* 19, 2 (2017), 408–417.

[24] Rundong Tian, Christine Dierk, Christopher Myers, and Eric Paulos. 2016. MyPart: Personal, Portable, Accurate, Airborne Particle Counting. In *Proceedings of the 2016 CHI Conference on Human Factors in Computing Systems, San Jose, CA, USA*. 1338–1348.

[25] Sotiris Vardoulakis, Bernard EA Fisher, Koulis Pericleous, and Norbert Gonzalez-Flesca. 2003. Modelling air quality in street canyons: a review. *Atmospheric environment* 37, 2 (2003), 155–182.

[26] Dejun Yang, Guoliang Xue, Xi Fang, and Jian Tang. 2012. Crowdsourcing to smartphones: incentive mechanism design for mobile phone sensing. In *The 18th Annual International Conference on Mobile Computing and Networking, Istanbul, Turkey*. 173–184.

[27] Jing Yuan, Yu Zheng, and Xing Xie. 2012. Discovering regions of different functions in a city using human mobility and POIs. In *Proceedings of the 18th ACM SIGKDD international conference on Knowledge discovery and data mining*. ACM, 186–194.

[28] Chao Zhang, Junchi Yan, Changsheng Li, Xiaoguang Rui, Liang Liu, and Rongfang Bie. 2016b. On Estimating Air Pollution from Photos Using Convolutional Neural Network. In *Proceedings of the 2016 ACM Conference on Multimedia Conference, Amsterdam, The Netherlands,*. 297–301.

[29] Xinglin Zhang, Zheng Yang, Wei Sun, Yunhao Liu, Shaohua Tang, Kai Xing, and XuFei Mao. 2016c. Incentives for Mobile Crowd Sensing: A Survey. *IEEE Communications Surveys and Tutorials* 18, 1 (2016), 54–67.

[30] Zheng Zhang, Huadong Ma, Huiyuan Fu, Liang Liu, and Cheng Zhang. 2016a. Outdoor Air Quality Level Inference

via Surveillance Cameras. *Mobile Information Systems* 2016 (2016), 9825820:1–9825820:10.
[31] Zheng Zhang, Huadong Ma, Huiyuan Fu, and Xinpeng Wang. 2015. Outdoor Air Quality Inference from Single Image. In *21st International Conference on MultiMedia Modeling, Sydney, NSW, Australia,*. 13–25.
[32] Yu Zheng, Furui Liu, and Hsun-Ping Hsieh. 2013. U-Air: when urban air quality inference meets big data. In *The 19th ACM SIGKDD International Conference on Knowledge Discovery and Data Mining, Chicago, IL, USA*. 1436–1444.

Received August 2017; Revised November 2017; Accepted January 2018